# Syn-Depositional Halokinesis in the Zechstein Supergroup (Lopingian) Controls Triassic Minibasin Genesis and Location

Amir Joffe [1*], Christopher A-L. Jackson[1,2], Leonardo M. Pichel[3]

1. Basins Research Group (BRG), Department of Earth Science and Engineering, Imperial College London, South Kensington Campus, SW7 2BP, UK
2. Jacobs, Manchester, M15 4GU, UK
3. Department of Earth Science, University of Bergen, Allégaten 41, 5007, Bergen, Norway

## Abstract

Salt tectonics is typically caused by the flow of mobile evaporites in response to post-depositional gravity gliding and/or differential loading by overburden sediments. This situation is considerably more complex near the margins of salt basins, where carbonate and clastic rocks may be deposited at the same time and interbedded with more mobile evaporitic strata. In these cases, syn-depositional salt flow may occur due to density differences in the deposited lithologies, although our understanding of this and related processes is relatively poor. We here use 3D seismic reflection and borehole data from the Devil's Hole Horst, West Central Shelf, offshore UK to understand the genesis, geometry and kinematic evolution of intra-Zechstein Supergroup (Lopingian) minibasins and their effect on post-depositional salt deformation. We show that immobile, pinnacle-to-barrier-like, carbonate build-ups and anhydrite are largely restricted to intra-basin highs, whereas mobile halite, which flowed to form large diapirs, dominates in the deep basin. At the transition between the intra-basin highs and the deep basin, a belt of intra-Zechstein minibasins occur, forming due to the subsidence of relatively dense anhydrite into underlying halite. Depending on primary halite thickness, these intra-Zechstein

minibasins created topographic lows, dictating the position for nucleation and subsequent down-building of Triassic minibasins. Our study refines the original depositional model for the Zechstein Supergroup in the Central North Sea, with the results also helping us better understand the style and distribution of syn-depositional salt flow on other layered evaporitic sequences and the role intra-salt heterogeneity and related deformation may have in the associated petroleum plays.

## Introduction

Salt tectonics occurs in over 100 sedimentary basins worldwide and is responsible for the formation of a remarkably complex range of structures (see Jackson & Hudec, 2017). These structures are important, given they can strongly influence the tectonostratigraphic evolution and petroleum system development of these basins. Most studies focus on the structural styles and stratigraphic patterns related to post-depositional salt flow; i.e. the post-depositional mobilization of the salt in response to differential sediment loading, gravity gliding and/or thick-skinned tectonics (Talbot & Jackson, 1987; Peel et al., 1996; Volozh et al., 2003; Hudec and Jackson, 2004; Brun and Maunduit 2008, 2009; Quirk et al., 2012; Fernandez et al., 2017; Pichel et al., 2018; Jackson et al., 2019). In these studies, the timing and style of salt flow is typically recorded by deformation and stratigraphic patterns within the seismically well-imaged, supra-salt sedimentary sequences (Jackson and Hudec, 2017). Conversely, much less is known about the drivers and consequences of syn-depositional salt flow, for example how the syn-depositional salt flow related to the primary lithology distribution within Layered Evaporite Sequence (LES) (Rowan et al., 2019), what types of intra-salt structural styles form because of this relatively early movement, or how syn-depositional movement impacts subsequent post-depositional salt flow and related deformation. Our lack of knowledge of these processes and their products possibly reflects the fact that evidence for syn-depositional salt flow is often harder to obtain, given the difficulties associated with the imaging of internal (i.e., intra-salt) structure and stratigraphy of salt bodies on seismic reflection data (see Jones and Davison, 2014). However, modern 3D seismic reflection data can occasionally image intra-salt layering and complex intra-salt deformation patterns (e.g., Central North Sea, offshore UK; Van Gent et al., 2011; Cartwright et al., 2012; e.g., Santos Basin, offshore Brazil; Gamboa et al., 2008; Davison et al., 2012 Fiduk and Rowan, 2012; Dolley et al., 2015; Jackson et al., 2015; Pichel et al., 2019; e.g., the Levant Basin; Gvirtzman et al., 2013). In some of these examples, the relative timing between salt deposition and deformations is debatable, principally due to intense post-depositional salt flow and diapirism obscuring the evidence of earlier intra-salt structures and stratigraphic patterns (i.e. thickness changes, onlaps) (Gamboa et al., 2008; Davison et al., 2012; Dooley et al., 2015; Fiduk & Rowan, 2012).

In the Central North Sea, offshore eastern UK, syn-depositional salt flow was originally described in the Zechstein Supergroup (Clark et al., 1998) (Figure 1). These authors show several 2D seismic profiles characterising the seismic expression and structural style of intra-Zechstein, syn-depositional minibasins, which they refer to as 'rafts'. Additionally, using vintage 3D seismic reflection data they produce a series of thickness maps to illustrate how a single intra-salt minibasin evolved, showing that the depocenter location was not fixed, but instead shifted through time (Figure 1C, 1D). Several mechanisms were proposed by Clark et al. (1998): (1) thin skinned extension triggered by basin-forming regional tilting; (2) syn-Zechstein basement fault activation; (3) syn-Zechstein basement-induced shortening; (4) differential loading created by shelf progradation; (5) gravity collapse due to density variations between the halite/carbonate/anhydrite units; and (6) dissolution collapse. The authors conclude these pre-Triassic, intra-Zechstein 'rafts', were most likely created by the combination of two mechanisms: (i) thin-skinned extension which was triggered by regional tilt; and (ii) sediment supply, which filled the accommodation created by the down-dip (i.e., basinward) flowing halite. How this behaviour related to the growth of adjacent salt structures and subsidence patterns in nearby minibasins was not discussed.

Here we expand on these ideas initially formulated by Clark et al. (1998) by using modern, 3D seismic reflection and borehole data from the eastern flank of the Devil's Hole Horst, UK Central North Sea (Figure 1A). Our study area is marked by spatial changes in the lithology and overall thickness of the Zechstein Supergroup. This location, coupled with minimal post-depositional deformation and high-resolution seismic imaging, make the southern corner of the Devil's Hole Horst a prime area to revisit this under-explored aspect of salt-tectonic (Figure 1A). By integrating 3D seismic reflection data and well data, we can: (1) characterize and map syn-depositional, salt-related deformation within the Zechstein Supergroup; (2) relate the structural style of syn-depositional minibasins to primary lithological variations within the salt; and (3) explore how the syn-depositional salt flow influenced post-depositional salt and overburden deformation.

## Geological Setting

Cisuralian (Early Permian) rifting, associated with the development of the Central Graben, influenced the location and extent of the Zechstein Supergroup evaporites (Ziegler, 1975; Hodgson et al., 1992). During the early stages of rifting, subsidence rates exceeded sediment accumulation rate, forming a sediment starved, intra-continental basin (Hodgson et al., 1992; Glennie & Underhill, 1998). A marine transgression during the Guadalupian (Middle Permian) resulted in desert lakes filling the rift-related relief, which when coupled with limited influx of marine seawater, enabled the development of hyper-saline conditions and the deposition of evaporite-bearing sedimentary sequences (Smith, 1979; Ziegler, 1989; Glennie & Underhill, 1998; Taylor, 1998). More specifically, four to five cycles of flooding and evaporation during the Lopingian (Late Permian) resulted in the deposition of a LES known as the Zechstein

Supergroup (Smith et al., 1993; Armour et al., 2004). Repeated flooding and evaporation directly influenced lithological distribution in the Zechstein Supergroup, i.e., carbonate- and anhydrite-rich units were deposited at the basin margins and on intra-basin structural highs during highstands, whereas halite- and K-Mg-rich salt-rich units were deposited in the deeper basins during lowstands (Tucker, 1991).

A second pulse of rifting during the Early Triassic reactivated the basement-involved, sub-salt faults, triggering post-depositional flow and reactive rise of the overlying Zechstein Supergroup salt (Jackson et al., 2019). In the halite-rich DZ3 and DZ4, stocks and N-trending salt walls formed. Triassic salt tectonics resulted in relatively thick sequences of nonmarine Triassic rocks being contained within minibasins; these sequences thin towards and onlap flanking salt bodies (Ziegler, 1975). Later Jurassic rifting had limited effect on diapiric rise due diapir welding, even if the extension could cause some diapiric collapse. Cretaceous and post-Cretaceous post-rift shortening was restricted to the basin axis and did not squeeze and thus rejuvenate diapirs on the basin flanks. The salt related structures studies here thus retain their primary geometry.

Based on the percentage of halite found in boreholes and inferred from salt-related structural styles imaged in seismic reflection data, the Zechstein Supergroup is divided into four depositional zones (DZ) (sensu Clark et al., 1998) (Figure 1A, 1B). DZ1 is located above intra-basin structural highs, and consists mainly of shelfal carbonate, anhydrite, and clastic rocks, with little or no halite (<10%). DZ2 is similar to DZ1 but contains a higher percentage of halite (10-50%), whereas DZ3 is characterized by relatively minor amounts of shallow waters shelfal rocks and a larger proportion of halite (50-80%). DZ2 and DZ3 together define the transition from the basin margin to basin centre, they typically deposited on and thus define basinward-dipping slopes (Clark et al., 1998; Patruno et al., 2018; Grant et al., 2019; Jackson et al., 2019). These basinward dipping slopes formed due to thermal subsidence in the axis of the North Sea, following and during Permian rifting. 3D seismic-based analysis of the Mid-North Sea High by Patruno et al. (2018) indicate that this transitional region may be composed of a hybrid sulphate-carbonate platform (termed Z1-2; following Taylor, 1998), capped by a thin, carbonate platform (termed Z3 following Taylor, 1998). Using the terminology of Clark et al. (1998), we would therefore assign the Mid-North Sea High region to DZ1 or DZ2. Finally, the deep basinal areas are defined by DZ4, which consists almost entirely of halite (>80%). In this zone diapirs and deep minibasins represent the main salt-tectonic structures; in contrast, DZ1 and DZ2 are largely undeformed or only weakly deformed due to the lack of mobile salt (Clark et al., 1998; Jackson et al., 2019).

## Data and Methodology

We use a 1460 $km^2$ pre-stack time-migrated 3D seismic volume, that covers Zechstein Supergroup DZ2- DZ4 (Figure 1). The seismic reflection data were collected in 2012 and processed in 2014. The final bin-size was 12.5 x 12.5 m, with a dominant frequency of 25 Hz at depth of interest. This approximates to a vertical seismic resolution of ~50 m seismic vertical resolution at the depth of interest, using an average interval velocity of 4916 m/s extracted from the sonic log from borehole 28/5-1. The data is zero-phase processed with SEG ‘reverse’ polarity, where a downward increase of acoustic impedance is represented by a negative (trough; blue) and positive (peak; red) seismic reflection event, respectively. The dataset is in the NE portion of Quadrant 28 on the United Kingdom Continental Shelf (UKCS), adjacent to areas in which Clark et al. (1998) documented the syn-depositional flow and deformation of Zechstein Supergroup salt (Figure 1A). Six wells were also available for this study; two wells are in DZ3 (28/9-4 & 28/4a) and four in DZ4. In our dataset, the lithology of DZ1 and DZ2 are not constrained by wells and must thus be inferred from the prevailing salt-related structural style (see Clark et al., 1998; Jackson et al., 2019). Two wells (28/4a-2 & 28/5-1) are only c. 10 km apart, allowing us to constrain the boundary between DZ3 and DZ4 with relative precision (Figure 1A).

We use well-logs to determine the current lithological variations within the Zechstein Supergroup, given that post-depositional flow of the unit has undoubtedly modified the original lateral and vertical (i.e., stratigraphic) distribution of the main rock types. More specifically, it is likely that redistribution of the primary lithologies was rheologically controlled, with more mobile halite and potash salt flowing more readily then less mobile clastic, anhydrite, and carbonate rocks, such as those encountered at the base of the Zechstein Supergroup. (Jackson et al., 2015). However, by considering: (i) the current lithological variability of the Zechstein Supergroup in the context of its seismically imaged structural style and inferred kinematic development; and (ii) other regional studies of the Zechstein Supergroup (Clark et al., 1998; Jackson and Stewart, 2017; Jackson et al., 2019; Grant et al., 2019), we can infer the original composition of the Zechstein Supergroup. Well data were also used to constrain the age of four regional seismic horizons (base and top Zechstein, top Triassic, top Jurassic), and one intra-salt horizon, which we mapped across the dataset (Figure 2).

The base and top Zechstein Supergroup reflections define the key salt-bearing interval, whereas the locally mappable intra-salt reflection separates weakly reflective, halite-rich sequences below from more reflective, halite-poor sequences above (see below). This distinction becomes important later when discussing seismic-stratigraphic evidence for syn-depositional salt flow. Confidently discriminating between syn- and post-Zechstein deformation is difficult, given salt-related deformation was protracted, initially being driven by intra-Zechstein Supergroup density differences between halite-anhydrite/carbonate, and then by evaporite-clastic differences in density between the Zechstein Supergroup and Triassic. Notwithstanding this challenge, we define the initial phase (i.e., syn-Zechstein Supergroup) of deformation by identifying intra-formational onlaps and downlaps within the Zechstein Supergroup, between units with markedly different seismic character. We then define the subsequent phase of deformation by identifying Triassic onlap onto salt structures, in particular diapirs. Due to its relatively uniform, clastic-dominated lithology, the Triassic minibasins are very weakly reflective, whereas the overlying lithologically more heterogeneous Jurassic interval is very reflective (Figure 3).

# Results

## Composition of the Zechstein Supergroup

We determined the composition of the Zechstein Supergroup using well-log data. Two wells (28/4a-2 & 28/5-1) penetrated and logged the entirety of the Zechstein Supergroup, whereas the other four penetrated and logged only its upper portion. The former two wells prove a 30-50 m thick carbonate layer at the base of the otherwise evaporite-rich sequence (Figure 3). This basal carbonate-rich unit characterises the Zechstein Supergroup across much of the North Sea, recording the temporal transition from the non-marine environment recorded by the Rotliegend Group to the more restrictive marine conditions in which the Zechstein was deposited (Glennie & Underhill, 1998; Brackenridge et al., 2020). Well 28/5-1, which penetrates a diapir in DZ4 (c. 90% halite), shows an abrupt upward transition from the carbonate layer into a thick (650 m) halite interval, whereas the basal carbonate in well 28/4a-2 is separated from the overlying halite unit (c. 60% of the total penetrated thickness) by a thin (c. 25 m), claystone-bearing unit. In all wells the Zechstein Supergroup is capped by a 25-90 m thick anhydrite-dominated unit that is locally interbedded with thin (5-10 m) layers of claystone (Figure 3). Based on its apparent predominance to areas of inflated salt (i.e., diapir crests), we infer that this unit represents crestal caprock formed by the preferential dissolution of halite and other soluble rock types like potash salts, with the claystone possibly representing insoluble clastic material that originally accumulated within the depositional sequence (e.g., Ulrich et al., 1984; Warren, 2006). Halite dominates the core of the underlying diapirs, as proven by 28/5-1 and 28/4a-2 (Figure 3).

## Zechstein Supergroup Structural Framework

The base Zechstein surface has a convex-to-the-basin plan-view geometry that broadly dips eastwards (Figure 4A). This convex shape reflects the study area's location on the eastern flank of Devil's Hole Horst (Figure 1A). We also note that this shape mimics the boundaries between the depositional zones mapped by Clark et al. (1998) (Figure 1A). The rest of the base Zechstein surface is relatively smooth, dipping east, although an E-W striking, N-dipping fault occurs in the north-eastern part of the dataset (Figure 4A). Other structures observed on the base Zechsterin surface are geometrically similar to those identified directly above on the top Zechstein Supergroup surface (i.e., Figure 4A), suggesting they are geophysical artifacts related to velocity pull-ups.

In a similar manner to the base Zechstein surface, the top Zechstein surface also dips eastwards. The surface is, however, not smooth, but instead is defined by numerous salt diapirs, the most prominent of which are two broadly curvilinear, sub-parallel, convex-into-the-basin salt walls (SW1&SW2; Figure 4B&C). These walls are 1.5-7 km wide, 150-500 ms tall, and at least 30 km long, extending northwards and southwards outside of the dataset. SW1 has well-defined, smooth margins but SW2 is more amorphous, being characterized by several W-trending, spur-like walls that protrude from its eastern margin (Figure 4C). We observe shorter protrusions, with a similar easterly trend, along the eastern edge of SW1. The salt walls are separated by minibasins that are, between SW1 and SW2, broadly N-trending, elongate, and convex-into-the-basin, like their bounding diapirs (MB2) (Figure 4C). The minibasin between the margin and SW1 (MB1) dies-out north-eastwards as the flanking salt walls merge to form a broader salt plateau (MB1; Figure 4C). MB2 and other minibasins in the southerly portion of SW2 contain isolated salt stocks that are 0.4-1.5 km in diameter and up to 500 ms tall (Figures 4D, 6).

## Intra-Zechstein Seismic Facies

We recognize four key seismic facies in the Zechstein Supergroup. The first is located mostly in the west of our study area and is marked by a distinct, high-amplitude, positive (red) reflection at the base of the Zechstein Supergroup, which defines several broadly mounded structures (Figure 7). The second is a seismically chaotic unit that is widespread at the base of the Zechstein Supergroup, and which defines the core of the most prominent salt structures, such as diapirs (Figures 5, 6). The third is defined by more continuous, moderate-amplitude reflections that occur almost exclusively in upper part of the Zechstein Supergroup, and which typically forms bowl-shaped packages that onlap and thin towards flanking diapirs (Figure 5, 7 – 9). Spatially, this seismic facies is restricted to the SE of the study area, mostly within DZ3 (as mapped by Clark et al. 1998) (Figure 1, 4E). The fourth seismic facies type is observed locally at the top of the Zechstein Supergroup and is defined by moderate- to high-amplitude reflections that onlap onto and/or dip away from broadly flat-topped diapirs (Figure 7B).

We interpret that the intra-salt reflectively and seismic facies changes in the Zechstein Supergroup marks an upward transition from a halite-rich, diapiric unit (proven by wells 28/5-1 and 28/4a-2; Fig. 2; cf., Jackson et al., 2015) to a more heterogeneous, anhydrite-dominated unit (Rodriguez et al., 2018). Based on its bowl-shaped external form, and the fact that internal reflections thin towards and onlap onto structures composed of the more chaotic seismic facies, we interpret that intra-salt reflectivity in the upper part of the Zechstein Supergroup define intra-salt minibasins, similar to those interpreted elsewhere in the Central North Sea (Clark et al., 1998; Jackson and Stewart, 2017). These intra-Zechstein minibasins are thinnest along the westerly part of the study-area and within MB1, and thicker to the southeast (Figure 4E). We also note that these minibasins may be perched along the flanks of the diapiric salt walls and, occasionally, encased within the walls themselves (Figure 4F).

Intra-Zechstein Structural Framework

To better understand the types and possible origins of the different styles of intra-Zechstein minibasins, we provide four examples of their structural and stratigraphic context using four cross-sections trending broadly east, parallel to the structural dip of the base Zechstein (Figure 4B).

*Section 1*

The first cross-section is located within DZ2 and DZ3 and reveals several broadly mounded structures at the base of the Zechstein (i.e., the first seismic facies) (Figure 7). These structures are capped by a distinct high-amplitude positive (red) reflection that continue westwards, towards the basin margin. The mounds form a series of approximately NNW-trending, 200-300 m-wide, up to 200 ms-tall (i.e., up to 983 m-thick, based on the average interval velocity of 4916 m/s extracted from the 28/5-1 sonic log), crescentic features (south in Figure 7B), or lower-relief, more amorphous features (north in Figure 7B). These mounds are overlain by the other three key seismic facies described above (i.e., halite-rich diapiric salt; deep pink in Figure 7A&C, an anhydrite-rich minibasin; light pink in Figure 7A&C, and carbonate rich units at the base and top of the Zechstein Supergroup; light blue in Figure 7A&C). The second locally onlaps the largest mounded structure at the base of the Zechstein Supergroup on the eastern side of the section, with the third seismic facies type observed at the top of the Zechstein Supergroup (Figure 7A). In the centre of the section, the diapir is the same hight of and has similar geometry to the other two diapirs but is associated with a soft (trough) blue reflection which onlaps onto the western diapir, and is onlapped by the third seismic facies to the east.

Based on their mounded geometry and seismic expression (Figure 7C), the abundance of carbonates at the base of the Zechstein Supergroup as demonstrated by wells (Figure 3), and their tectono-stratigraphic context at the evaporitic basin margin, we interpret these base-Zechstein features as carbonate build-ups (Figure 7A&C). These features are in an area previously identified by Clark et al. (1998) as being carbonate-rich, further supporting our interpretation. Similar carbonate-related features are documented in the Southern North Sea (Grant et al., 2019). Given the description above, we infer these soft reflection at the top of the central diapir are carbonate dominated. The differences in the seismic expression between the basal and top carbonate units (i.e., first and forth seismic facies) could be related to: (i) the carbonates being lithologically and thus petrophysically distinct, thereby differing in terms of their density and velocity; and/or (ii) the carbonate are lithologically and thus petrophysically similar, but are overlain by different strata (e.g., Jurassic sandstone or mudstone) that define either a downward increase in acoustic impedance and thus negative rather than positive, top-salt reflection.

*Section 2*

The second cross-section is located mostly within DZ3. The most prominent features in this section are the large, halite-rich diapirs (Figure 8). Small (150 ms tall by 1000 m wide), triangular-shaped and generally more reflective bodies also occur locally at the base of the Zechstein Supergroup. These bodies are onlapped and/or downlapped by highly reflective, sigmoidal, clinoform-like reflections (Figure 8). These highly reflective sigmoidal reflections are thickest adjacent to the large diapir to the east, onlapping its western flanks, forming an asymmetric minibasin that is welded to the sub-salt strata (Figure 8B). Based on the more pronounced thickness variations, truncations, and onlaps within the Zechstein Supergroup relative to the Triassic minibasin which lies above, we infer that most of the salt flowed into the diapir during the Permian, before Triassic deposition. However, salt continued to flow during the Triassic, such that it affected thickness patterns in the lower parts of the minibasin (Figure 8B). Where present, minor thickness variations in the Triassic minibasin mirror the thickness variation in the intra-Zechstein packages (Figure 4E&H). We identify another relatively small (200 ms thick), intra-salt minibasin in the centre of the cross-section (Figure 8A).

*Section 3*

The third cross-section shows two relatively thin (200-250 ms), bowl-shaped packages of semi continuous, intra-Zechstein reflections perched within a large salt wall (SW3; Figure 9A). These packages thin towards and onlap onto flanking diapirs (Figure 9A). A similar, albeit highly asymmetric sequence is also present dipping eastwards on the eastern flank of the large wall and being overlain and indented by a small, Triassic minibasin (Figure 9A). Across the section, Jurassic strata are broadly tabular and generally sub-horizontal, locally thinning across and onlapping onto Triassic minibasins where these protrude above the top salt (Figure 9). We suggest that the easterly dips within the easternmost intra-Zechstein minibasin was caused by the subsequent subsidence of Triassic clastic strata down into the salt, which caused tilting of the previous deposited evaporitic rocks (Figure 9B).

*Section 4*

Unlike the previous examples, the fourth and final example is in the southern part of the dataset (Figure 4B). This area is characterised by higher density of intra-Zechstein minibasins, and higher structural complexity (Figure 4E). In this example, two Triassic minibasins are present (MB1 and MB2) and separated by two salt walls (SW1 and SW2) (Figure 5). The broad bowl-shaped intra-Zechstein sequence below MB1 is relatively thin (150 ms), symmetrical in cross-section (Figure 5) and elongate in map-view (Figure 4C). The intra-Zechstein minibasin below MB2 is thickest on the flanks of SW2, thinning towards both the crest of the diapir and updip towards the base of SW1. The Triassic minibasin MB2 is thickest where the intra-Zechstein minibasin onlaps SW2 (Figure 5).

Based on thickness relationships between the intra-Zechstein minibasin below MB2 and the Triassic minibasin, we interpret that the post-Zechstein subsidence of Triassic minibasins into the underlying salt caused the intra-Zechstein minibasins to rotate south-eastwards (Figure 5B). We generally observe more complex deformation in the southern part of the study area. In particular, we see more evidence for tilting of intra-Zechstein minibasins due to the subsidence of younger, Triassic minibasins. The reason for this is not clear, but it might reflect the fact that in this region, down-flank of the Devil's Hole Horst, mobile halite was thicker and, therefore, there was still material to be evacuated from below the intra-Zechstein minibasins when the Triassic minibasins formed.

### Triassic

The Triassic is mostly weakly reflective and chaotic, although it is locally defined by low-amplitude, moderately continuous reflections. Where observed, these reflections/packages define broadly isopachous intervals that may onlap the diapir flanks (Figures 5, 6, 8). The relatively smooth (compared to the top-salt), regionally consistent eastward dip observed at the top Triassic level (Figure 4E) indicates that salt-related deformation peaked during the Lopingian-Early Triassic and declined during the Late Triassic-Early Jurassic. Other structures superimposed on the generally consistent eastward dip relate to continued salt flow during the Triassic. Circular depressions are common, located above individual salt-stocks; these could potentially be related to the dissolution of the crests of salt diapirs piercing this interval and/or diapir collapse related to post-Triassic extension and diapir widening (Mannie et al., 2014).

## Interpretation and Discussion

## Syn-depositional salt-related deformation and controls on subsequent structural style

Our 3D seismic reflection data from the eastern flank of the Devil's Hole Horst, UKCS, show that the Zechstein Supergroup has a complex seismic-stratigraphic architecture. At the base of the Zechstein Supergroup, well-data prove a basal carbonate build-up, which are also seen at the seismic reflection data as mounded structures, and protruding carbonate platforms (e.g., Figure 5 & 7). Semi-continuous, moderate-amplitude seismic reflection onlap and dip away from weakly reflective, chaotic, sub-circular-to-elongate bodies. Well data also show that the Zechstein Supergroup is lithologically heterogeneous, comprising of carbonate, halite, and anhydrite. Based on these observations, we interpret that the reflective packages are intra-Zechstein minibasins, whereas the chaotic bodies are diapirs. Although they are not penetrated by wells, we infer that the minibasins are anhydrite-rich, whereas wells prove that the diapirs comprise predominantly halite. Critically, the seismic-stratigraphic architecture of the Zechstein Supergroup argues for pre-Triassic salt flow, adjacent to and/or overlying basal carbonate build-ups. Similar observations and interpretations were made by Clark et al. (1998), who originally mapped these features to the North and North-West of our study area.

We therefore argue that although the Zechstein Supergroup depositional model of Clark et al. (1998) accurately captures the basin-scale distribution of the key rock types, because of its more regional focus, and the data quality and quantity at that time, it does not demonstrate how the variable density and mechanical properties of these rocks controlled syn- and post-depositional salt flow and related deformation.

Here, we propose an update to the idealized model of Clark et al. (1998), by incorporating both the structural and lithological variability observed within the Zechstein Supergroup in our study-area (Figure 10). Our model envisages the same four main Zechstein Supergroup depositional cycles and zones defined by Clark et al. (1998), with each cycle and zone consisting of an initial carbonate deposition associated with marine transgression and basin flooding, followed by the deposition of anhydrite, and then halite during basin desiccation.

Deposition during the first cycle (i.e., carbonate, anhydrite and then halite) occurs across the generally smooth, basinward-dipping, base-Zechstein Supergroup surface. During this time, there is no gravitational potential or significant vertical density variations to drive salt flow and related deformation (Figure 10A). The second cycle starts with deposition of relatively dense carbonate at the basin margin, on top of less dense halite (Figure 10A). The deposition of dense carbonates and subsequent anhydrite on top of less dense and more mobile halite triggers down-dip salt evacuation, inflation, and diapirism of the latter (Figure 10B). The second cycle ends with the deposition of a second halite unit, coeval to the downdip flow, inflation and diapirism of the previous halite unit (Figure 10C). The third cycle is also characterised by the deposition of a basin-margin, carbonate-dominated unit (Figure 10D). Assuming the basinward flow of halite during the preceding phases was sufficient to generate a local, salt-cored structural high, the near-margin area may have been sufficiently shallow to allow the nucleation of shallow-water carbonates (Figure 10D). This element of the model is supported by the first example seen in Figure 7, which suggest that locally at least, carbonate build-ups could form on areas of inflated, halite-rich salt, at some distance into the basin. The third cycle continues with deposition of anhydrite (Figure 10E) followed by halite (Figure 10F). During deposition of these evaporitic cycles, mobile halite deposited during previous cycles continued to flow down-dip due to loading at the basin-margin by dense, carbonate-/anhydrite-rich units (Figure 10E, 10F). By the fourth cycle (Figure 10G), a progradational carbonate platform developed along the basin margin, as observed in Figure 5, passing laterally basinward into anhydrite-rich minibasins surrounded by halite-rich salt walls.

The variability of halite proportion in each cycle governs the magnitude and location of salt-related deformation during Zechstein Supergroup deposition. The final halite thickness and proportion in each cycle also influenced the style and intensity of post-depositional (i.e. post-Lopingian) salt-related deformation (Figure 10H). In areas where the LES was halite-rich and relatively thick, post-depositional salt flow was substantial, allowing large diapirs to form; in contrast, in areas where the LES mobile halite was relatively thin and impure, post-depositional deformation were less pronounced (Figure 4H). These differences in the magnitude of deformation, governed by the amount and proportion of halite in the different cycles, are seen in our dataset, which is highlighted by the different cross-section examples (Figures 7-9). For example, carbonate deposition at the basin margin promoted the syn-depositional basinward expulsion of mobile evaporites, favouring the development of larger Triassic minibasins above the anhydrite-dominated intra-Zechstein minibasins, lateral to the mechanically stronger carbonates (e.g., Figure 7). We also note that thickness changes in the Triassic minibasins mirror those in the intra-Zechstein, suggesting that subtle topographic lows above intra-Zechstein minibasins localised earliest Triassic deposition, thus triggering the nucleation and dictating the position of the Triassic minibasins (e.g., Figure 4F&8). Conversely, where intra-Zechstein minibasins were small relative to their flanking salt walls, they did not act as nucleation sites for subsequent Triassic minibasins (e.g., Figure 9). Finally, we show that thicker (and generally larger) intra-Zechstein minibasins are preferentially formed where the mobile halite was initially thicker, in the deep basin (e.g., Figure 5).

In addition to being genetically related to the intra-Zechstein minibasins, the subsidence history of the Triassic minibasins may have been controlled by the older structures. For example, the Triassic minibasins contain strata units that are wedge- rather than bowl-shaped, which we infer minibasin tilting during subsidence (e.g. Figure 5) (Rowan & Weimer, 1998; Jackson et al., 2019). The reason for this is not clear, but it may reflect the fact that Triassic minibasins impinged on the underlying Zechstein minibasin as they subsided, with the latter containing relatively rigid, largely immobile anhydrite flanked by more mobile halite. Such similar interactions between intra-salt and supra-salt were observed in the Precaspian Basin (Fernandez et al., 2017), where encased intra-salt minibasins dip towards the supra-salt minibasins as a consequent of loading by the younger minibasin strata (see Figures 12 and 15 in their text). As such, our conceptual model may be more broadly applicable to other basin-margin and intra-basin high positions in the Zechstein salt basin, as well as comparable locations in other global salt basin containing layered evaporite sequences (see below).

## Syn depositional salt flow in other salt basins

The results of our study of Lopingian salt in the North Sea have more general, broader implications for understanding salt tectonics and related petroleum systems development in other salt basins. For example, in the Precaspian Basin, Kazakhstan, numerous, very large (up to 3 km-thick), Permo-Triassic, syn-depositional, intra-salt minibasins are encased in thick, Kungurian (Lower Permian) salt. Well data from the Precaspian indicate that these intra-salt basins contain clastic, carbonate, and evaporite (i.e., halite, anhydrite) rocks (Fernandez et al., 2017). The authors suggest that the large proportion of relatively dense anhydrite and carbonate within these minibasins was a key reason for their relatively quick encasement, confirming the importance of vertical (i.e., stratigraphic) lithology and density variations in driving density-driven subsidence. A notable difference between the North Sea and Precaspian examples is that in the former case, syn-depositional minibasins were not encased, likely reflecting the fact they nucleated above and subsided into an overall thinner, mobile, lower halite. Lateral (i.e., areal) variations in lithology and thus density likely also play a key role in determining when and where syn-depositional salt flow might occur. For example, in the North Sea and Precaspian Basin, relatively early (i.e., syn-depositional) salt flow and tectonics occur towards the basin margin in a transitional zone where mobile halite-rich sequences and denser, less-mobile halite-poor sequences are interbedded (Tucker, 1991). We thus propose that early, syn-depositional, sedimentary load-driven salt tectonics likely occurs in comparable settings in LES deposited in other salt basins, i.e., in near-basin margin areas characterised by the most pronounced lithological heterogeneity.

Syn-depositional salt flow within LES is documented in the Levant Basin, offshore Israel (Gvirtzmann et al., 2013), and has been argued for in the Santos Basin, offshore Brazil (Davison et al., 2012, Bose and Sullivan, 2022; see, however, a competing hypothesis presented by Jackson et al., 2015). However, in these cases, early deformation and accommodation was driven by gravity-gliding and contraction of the entire evaporite sequence, and not sediment loading. Because of this, this style of early salt tectonics is not restricted to the basin margin like the load-driven examples presented above but can instead occur anywhere within the basin where contraction occurs (e.g., the distal part of a salt-detached passive margin or above a base-salt step in a relatively proximal position; e.g., Dooley et al., 2016; Erdi and Jackson, 2021). In addition, recent numerical models show that syn-depositional deformation can also occur during the final stages of rifting, in a lithologically homogenous evaporite sequence lacking of an intra-salt density difference. In this case, syn-depositional minibasin formation likely occurs due to stretching-driven flow of salt (Pichel et al., 2022).

Regardless of the location in which it occurs and its origin, a key question is, therefore, “how do we distinguish intra-salt structural styles and thickness changes related to syn-depositional salt flow from those related to post-depositional deformation?” (see discussion in Allen et al., 2016). Clearly, information on the regional geological context (e.g., to determine regional events that may be responsible for driving salt tectonic-related deformation) and a combination of high-quality 3D seismic and borehole data (e.g., to clearly image and lithologically characterised the structures and stratigraphy of interest) are critical. For example, as suggested above, is the study area in a near-margin location, and are relatively similar proportions of halite-rich and halite-poor units encountered within the salt sequence? It is likely these conditions are met in other salt basins, but that subsequent salt tectonics (e.g., the growth of large diapirs and/or the formation of allochthonous salt bodies) meant that more subtle, earlier formed structures, such as syn-depositional minibasins are structurally overprinted or cannot be geophysically imaged. Our study area thus represents a “sweet-spot” within which these geometries are not only preserved, most likely due to the relatively thin, lower, mobile halite, but also imaged by seismic reflection data. Syn-depositional salt flow and early-formed evaporite minibasins may be more common than currently thought.

The results of our study have implications for petroleum exploration, and hydrogen ($H_2$) and carbon dioxide ($CO_2$) storage within the Southern North Sea and other salt basins. For example, carbonates at various stratigraphic levels within the salt could represent reservoirs, as observed in other parts of NW Europe (see review by Patruno et al., 2017), with syn-depositional deformation driving trap formation, and overlying halite acting as a seal. Reservoir quality within these units might vary downdip, with marginal grainstones passing basinward into rock types of lower reservoir quality, such as wackestones.” Depending on their permeability, extent, and connectivity these carbonates could, however, facilitate leakage of $CO_2$ stored in underlying, Rotliegned Group clastics, and they may impact the geometry and volume of caverns engineered to store $H_2$ (see review by Duffy et al., 2022).

## Conclusion

We here used modern 3D seismic reflection and borehole data from the eastern flank of the Devil’s Hole Horst, UK Central North Sea to provide seismic-stratigraphic evidence that minibasin downbuilding and diapirism occurred during deposition of the Zechstein Supergroup (i.e., syn-depositional salt tectonics). We illustrate four examples of intra-salt minibasins, characterised by different lithological variations and/or structural styles and discuss their influence on syn-depositional salt flow and subsequent, post-depositional deformation. Our first example shows how intra-Zechstein minibasins and halite-dominated diapirs develop away from the mechanically stronger, carbonate-dominated Zechstein rocks. We then showed how subtle topographic lows created by the intra-Zechstein minibasin control the nucleation of post-depositional Triassic minibasins. Finally, we demonstrate that in places where halite was still thick after the end of salt-deposition due to either (i) syn-depositional mobilization/inflation or (ii) halite-rich deposition towards the deep-basin, post-depositional minibasins were highly asymmetric. By integrating these observations, we propose a revised kinematic-depositional model that correlates intra-Zechstein lithological variability with syn-depositional salt deformation. We thus believe that our model is more broadly applicable to other areas of the Zechstein salt basin than the one originally proposed by Clark et al. 1998. Our model is also more applicable to layered evaporite sequences worldwide and may suggest that syn-depositional deformation is likely a more common phenomenon than often observed in areas affected by intense and long-lived post-depositional salt tectonics such as the Gulf of Mexico and South Atlantic. The results of this work have implications for hydrocarbon exploration and $CO_2$ sequestration in other salt basins, highlighting the structural and stratigraphic complexity which may occur in sequences classically considered only as seals.

## Acknowledgments

We would like to acknowledge TGS for permission to use the seismic reflection data shown in this study, in particular Annette Flethøj Tvedten and Will King. We would also like to thank Conor O'Sillivan, Ross Grant and Carl Fiduk for revieing this manuscript. Their imput was vital to this manuscript. We extend our thanks to the Schlumberger for their Petrel academic license to Imperial College London.

## References

Allen, H., Jackson, C. A.-L., & Fraser, A. J. (2016). Gravity-driven deformation of a youthful saline giant: the interplay between gliding and spreading in the Messinian basins of the

Eastern Mediterranean. *Petroleum Geoscience*, *22*(4), 340–356. https://doi.org/10.1144/petgeo2016-034

Armour, A., Evans, D., & Hickey, C. (2004). The Millennium A t l a s : petroleum geology of the central and northern North S e a THE MILLENNIUM ATLAS : of the Central and The project to produce the Millennium Atlas was organised by : *Petroleum Geology*

Booth, J. R., Dean, M. C., DuVernay, A. E., & Styzen, M. J. (2003). Paleo-bathymetric controls on the stratigraphic architecture and reservoir development of confined fans in the Auger Basin: central Gulf of Mexico slope. *Marine and Petroleum Geology*, *20*(6), 563–586. https://doi.org/https://doi.org/10.1016/j.marpetgeo.2003.03.008

Brackenridge, R. E., Underhill, J. R., Jamieson, R., & Bell, A. (2020). Structural and stratigraphic evolution of the Mid North Sea High region of the UK Continental Shelf. *Petroleum Geoscience*, *26*(2), 154–173. https://doi.org/10.1144/petgeo2019-076

Brun, J. P., & Mauduit, T. P. O. (2008). Rollovers in salt tectonics: The inadequacy of the listric fault model. *Tectonophysics*, *457*(1–2), 1–11. https://doi.org/10.1016/j.tecto.2007.11.038

Brun, J. P., & Mauduit, T. P. O. (2009). Salt rollers: Structure and kinematics from analogue modelling. *Marine and Petroleum Geology*, *26*(2), 249–258. https://doi.org/10.1016/j.marpetgeo.2008.02.002

Cartwright, J., Jackson, M., Dooley, T., & Higgins, S. (2012). Strain partitioning in gravity-driven shortening of a thick, multilayered evaporite sequence. *Geological Society Special Publication*, *363*(1), 449–470. https://doi.org/10.1144/SP363.21

Clark, J. A., Stewart, S. A., & Cartwright, J. A. (1998). Evolution of the NW margin of the North Permian Basin, UK North Sea. *Journal of the Geological Society*, *155*(4), 663. https://doi.org/10.1144/gsjgs.155.4.0663

Davison, I., Anderson, L., & Nuttall, P. (2012). Salt deposition, loading and gravity drainage in the Campos and Santos salt basins. *Geological Society, London, Special Publications*, *363*(1), 159 LP – 174. https://doi.org/10.1144/SP363.8

Dooley, T. P., Jackson, M. P. A., Jackson, C. A. L., Hudec, M. R., & Rodriguez, C. R. (2015). Enigmatic structures within salt walls of the Santos Basin-Part 2: Mechanical explanation from physical modelling. *Journal of Structural Geology*, *75*, 163–187. https://doi.org/10.1016/j.jsg.2015.01.009

Fernandez, N., Duffy, O. B., Hudec, M. R., Jackson, M. P. A., Burg, G., Jackson, C. A. L., & Dooley, T. P. (2017). The origin of salt-encased sediment packages: Observations from the SE Precaspian Basin (Kazakhstan). *Journal of Structural Geology*, *97*, 237–256. https://doi.org/10.1016/j.jsg.2017.01.008

Fiduk, J. C., & Rowan, M. G. (2012). Analysis of folding and deformation within layered evaporites in blocks BM-S-8 & -9, Santos Basin, Brazil. *Geological Society Special Publication*, *363*(1), 471–487. https://doi.org/10.1144/SP363.22

Gamboa, L. A. P., Machado, M. A. P., Da Silveira, D. P., De Freitas, J. T. R., Da Silva, S. R. P., Mohriak, W., Szatmari, P., & ANJOS, S. (2008). Evaporitos estratificados no Atlântico Sul: interpretação sísmica e controle tectono-estratigráfico na Bacia de Santos. *Sal: Geologia e Tectônica, Exemplos Nas Basicas Brasileiras*, 340–359.

Glennie, K. W., & Underhill, J. R. (1998). Origin, Development and Evolution of Structural Styles. In *Petroleum Geology of the North Sea* (pp. 42–84). https://doi.org/https://doi.org/10.1002/9781444313413.ch2

Grant, R. J., Underhill, J. R., Hernández-Casado, J., Barker, S. M., & Jamieson, R. J. (2019). Upper Permian Zechstein Supergroup carbonate-evaporite platform palaeomorphology in the UK Southern North Sea. *Marine and Petroleum Geology*, *100*, 484–518. https://doi.org/10.1016/j.marpetgeo.2017.11.029

Gvirtzman, Z., Reshef, M., Buch-Leviatan, O., & Ben-Avraham, Z. (2013). Intense salt deformation in the Levant Basin in the middle of the Messinian Salinity Crisis. *Earth and Planetary Science Letters*, *379*, 108–119. https://doi.org/10.1016/j.epsl.2013.07.018

Hodgson, N. A., Farnsworth, J., & Fraser, A. J. (1992). Salt-related tectonics, sedimentation and hydrocarbon plays in the Central Graben, North Sea, UKCS. *Geological Society, London, Special Publications*, *67*(1), 31 LP – 63. https://doi.org/10.1144/GSL.SP.1992.067.01.03

Hudec, M. R., & Jackson, M. P. A. (2004). Regional restoration across the Kwanza Basin, Angola: Salt tectonics triggered by repeated uplift of a metastable passive margin. *AAPG Bulletin, v*, *88*(7), 971–990. https://doi.org/10.1306/02050403061

Jackson, C. A. L., Jackson, M. P. A., & Hudec, M. R. (2015). Understanding the kinematics of salt-bearing passive margins: A critical test of competing hypotheses for the origin of the Albian Gap, Santos Basin, offshore Brazil. *Bulletin of the Geological Society of America*, *127*(11–12), 1730–1751. https://doi.org/10.1130/B31290.1

Jackson, C. A. L., Jackson, M. P. A., Hudec, M. R., & Rodriguez, C. R. (2015). Enigmatic structures within salt walls of the Santos Basin-Part 1: Geometry and kinematics from 3D seismic reflection and well data. *Journal of Structural Geology*, *75*, 135–162. https://doi.org/10.1016/j.jsg.2015.01.010

Jackson, C. A.-L., Duffy, O. B., Fernandez, N., Dooley, T. P., Hudec, M. R., Jackson, M. P. A., & Burg, G. (2019). The stratigraphic record of minibasin subsidence, Precaspian Basin, Kazakhstan. *Basin Research*, *0*(0), 1–25. https://doi.org/10.1111/bre.12393

Jackson, C. A.-L., & Stewart, S. A. (2017). Composition, Tectonics, and Hydrocarbon Significance of Zechstein Supergroup Salt on the United Kingdom and Norwegian Continental Shelves: A Review. *Permo-Triassic Salt Provinces of Europe, North Africa and the Atlantic Margins*, 175–201. https://doi.org/10.1016/B978-0-12-809417-4.00009-4

Jackson, C., Elliott, G. M., Royce-Rogers, E., Gawthorpe, R. L., & Aas, T. E. (2019). Salt thickness and composition influence rift structural style, northern North Sea, offshore Norway. *Basin Research*, *31*(3), 514–538. https://doi.org/10.1111/bre.12332

Jackson, M. P. A., & Hudec, M. R. (Eds.). (2017). Salt Tectonics. In *Salt Tectonics: Principles and Practice*. Cambridge University Press. https://doi.org/DOI: undefined

Jones, I. F., & Davison, I. (2014). Seismic imaging in and around salt bodies. *Interpretation*, *2*(4), SL1–SL20. https://doi.org/10.1190/INT-2014-0033.1

Mannie, A. S., Jackson, C. A.-L., & Hampson, G. J. (2014). Shallow-marine reservoir development in extensional diapir-collapse minibasins: An integrated subsurface case study from the Upper Jurassic of the Cod terrace, Norwegian North Sea. *AAPG Bulletin*, *98*(10), 2019–2055. https://doi.org/10.1306/03201413161

Patruno, S., Reid, W., Jackson, C. A.-L., & Davies, C. (2018). New insights into the unexploited reservoir potential of the Mid North Sea High (UKCS quadrants 35–38 and 41–43): a newly described intra-Zechstein sulphate–carbonate platform complex. *Geological Society, London, Petroleum Geology Conference Series*, *8*(1), 87. https://doi.org/10.1144/PGC8.9

Peel, F. J., Travis, C., & Hossack, J. (1996). Genetic structural provinces and salt tectonics of the Cenozoic offshore US Gulf of Mexico: A preliminary analysis. *AAPG Memoir*, *65*, 153–175.

Pichel, L. M., Finch, E., & Gawthorpe, R. L. (2019). The Impact of Pre-Salt Rift Topography on Salt Tectonics: A Discrete-Element Modeling Approach. *Tectonics*, *38*(4), 1466–1488. https://doi.org/10.1029/2018TC005174

Pichel, L. M., Peel, F., Jackson, C. A.-L., & Huuse, M. (2018). Geometry and kinematics of salt-detached ramp syncline basins. *Journal of Structural Geology*, *115*, 208–230. https://doi.org/https://doi.org/10.1016/j.jsg.2018.07.016

Quirk, D. G., Schødt, N., Lassen, B., Ings, S. J., Hsu, D., Hirsch, K. K., & Von Nicolai, C. (2012). Salt tectonics on passive margins: examples from Santos, Campos and Kwanza basins. *Geological Society, London, Special Publications*, *363*(1), 207–244. https://doi.org/10.1144/sp363.10

Rodriguez, C. R., Jackson, A.-L., Rotevatn, A., Bell, R. E., & Francis, M. (2018). Dual tectonic-climatic controls on salt giant deposition in the Santos Basin. *Brazil GEOSPHERE* |, *14*(1). https://doi.org/10.1130/GES01434.1

Rowan, M. G., Urai, J. L., Carl Fiduk, J., & Kukla, P. A. (2019). Deformation of intrasalt competent layers in different modes of salt tectonics. *Solid Earth*, *10*(3), 987–1013. https://doi.org/10.5194/SE-10-987-2019

Rowan, M. G., & Weimer, P. (1998). Salt-sediment interaction, northern Green Canyon and Ewing Bank (offshore Louisiana), northern Gulf of Mexico. *AAPG Bulletin*, *82*(5B), 1055–1082.

Smith, D. B. (1979). Rapid marine transgressions and regressions of the Upper Permian Zechstein Sea. *Journal of the Geological Society*, *136*(2), 155 LP – 156. https://doi.org/10.1144/gsjgs.136.2.0155

Smith, R. I., Hodgson, N., & Fulton, M. (1993). Salt control on Triassic reservoir distribution, UKCS Central North Sea. *Geological Society, London, Petroleum Geology Conference Series*, *4*(1), 547 LP – 557. https://doi.org/10.1144/0040547

Talbot, C. J., & Jackson, M. P. A. (1987). SALT TECTONICS. *Scientific American*, *257*(2), 70–79. https://doi.org/10.1038/scientificamerican0887-70

Taylor, J. C. M. (1998). Upper Permian—Zechstein. In *Petroleum Geology of the North Sea* (pp. 174–211). https://doi.org/https://doi.org/10.1002/9781444313413.ch6

Tucker, M. E. (1991). Sequence stratigraphy of carbonate-evaporite basins: models and application to the Upper Permian (Zechstein) of northeast England and adjoining North Sea. *Journal of the Geological Society*, *148*(6), 1019 LP – 1036. https://doi.org/10.1144/gsjgs.148.6.1019

Ulrich, M. R., Kyle, J. R., & Price, P. E. (1984). Metallic sulfide deposits in the Winnfield salt dome, Louisiana: evidence for episodic introduction of metalliferous brines during cap rock formation. In *Transactions, Gulf Coast Association of Geological Societies* (Vol. 34, pp. 435–422). GCAGS Transactions. https://doi.org/10.1306/ad4618b3-16f7-11d7-8645000102c1865d

Van Gent, H., Urai, J. L., & de Keijzer, M. (2011). The internal geometry of salt structures - A first look using 3D seismic data from the Zechstein of the Netherlands. *Journal of Structural Geology*, *33*(3), 292–311. https://doi.org/10.1016/j.jsg.2010.07.005

Volozh, Y., Talbot, C., & Ismail-Zadeh, A. (2003). Salt structures and hydrocarbons in the Pricaspian basin. *American Association of Petroleum Geologists Bulletin*, *87*(2), 313–334. https://doi.org/10.1306/09060200896

Warren, J. K. (2006). Evaporites: Sediments, resources and hydrocarbons. In *Evaporites: Sediments, Resources and Hydrocarbons*. https://doi.org/10.1007/3-540-32344-9

Ziegler, M. A. (1989). North German Zechstein facies patterns in relation to their substrate. *International Journal of Earth Sciences : Geologische Rundschau*, *78*(1), 105–127. https://doi.org/10.1007/BF01988356

Ziegler, P. A. (1975). Geologic Evolution of North Sea and Its Tectonic Framework1. *AAPG Bulletin*, *59*(7), 1073–1097. https://doi.org/10.1306/83D91F2E-16C7-11D7-8645000102C1865D

# Figure Captions

Figure 1: (A) Map showing the different depositional zones of the Zechstein Supergroup within the Central North Sea, as described by Clark et al., 1998. Highlighted are the 3D seismic surveys available for Clark et al., 1998 study and this study (zoomed area). Notice the dataset is located outside of the zone of syn-depositional salt flow as described by Clark et al., 1998. (B) Schematic cross-section describing an idealized deposition sequence of the Zechstein Supergroup through X-X' in A. (C) Cross-section through the one intra-Zechstein minibasin which was described in 3D by Clark et al. (1998). (D) Thickness maps of the sequences described in C are evidence for syn-depositional salt flow in the Zechstein Supergroup (Modified from Clark et al. (1998)).

Figure 2: Seismic well-tie for the 28/5a-2 well. We cannot fully constrain the intra-Zechstein minibasins lithology as no wells penetrated the intra-Zechstein minibasins in our dataset. This seismic well-tie holds the basis to the interpretation of our regional, supra-salt, horizons.

Figure 3: Well correlation panel through 5 of the 6 available wells flattened on Top Zechstein (for location see Figure 1A). Well logs available for this study either did not reach the well TD or were not available for the entirety of the well path. This is most apparent in the 28/9-4 and 28/5a-2 wells, which creates differences between well tracks (top) and geoseismic section (bottom). The former two wells prove a 30-50 m thick carbonate layers at the base of the otherwise evaporite-rich sequence. All wells show the presence of anhydrite and/or layered sequences of sedimentary facies at the top of the Zechstein Supergroup.

Figure 4: (A) Base-Zechstein Super Group structural map. A significant convex-to-basin shape is probably associated by the location relative to the Devil's Hole Horst (see Figure 1A for location). (B) Structural map of the top Zechstein Supergroup. Same curvilinear convex-to-basin is present, demonstrated by the salt walls architecture. (C) Location of the various salt walls (SW) and minibasins (MB) overlain on the top - Zechstein Supergroup structural map for

orientation. (D) Red circles indicate isolated salt stocks located within MB2 and beyond SW3, with few are located within SW3. White circles represent wells used in this study. (E) Thickness map of the intra-Zechstein minibasins, overlayed on a grey-scale Top Zechstein structural map. (F) Halite Thickness map, location of the intra-Zechstein (in Yellow) overlayed. (E) Top Triassic structural map not showing any clear indication for the curvilinear structures. (H) Triassic thickness map.

Figure 5: NW-SE trending seismic (above) and Geoseismic (below) profiles through the southern part of the dataset. Visible is the carbonate dominated margin of the Devil's Horst Hole (SW1). At the centre of the figure, a large Triassic minibasin caused the rotation of the intra-Zechstein minibasin. For location see Figure 3D.

Figure 6: Seismic cross section along the centre of MB2. Isolated salt stocks are trapped within the curvilinear minibasin. Intra-Zechstein reflection are also highlighted. For location see Figure 4B.

Figure 7: (A) W-E trending seismic and Geoseismic profiles through a carbonate-halite dominated intra-Zechstein minibasins. For location see Figure 3D. (B) Map of the top carbonate-rich interval at the base of the Zechstein Supergroup. (C) N-S trending seismic (above) and Geoseismic (below) profile through the carbonate-rich base-Zechstein buildups (for location see Figure 7B).

Figure 8: W-E trending seismic (above) and Geoseismic (below) profiles through the anhydrite-halite dominated intra-Zechstein minibasins. For location see Figure 3D.

Figure 9: W-E trending seismic (above) and Geoseismic (below) profiles through SW3 showing two symmetrical minibasins in its centre. For location see Figure 3D.

Figure 10: A revised depositional model for the Zechstein Supergroup along the eastern flank of Devil's Hole Horst showing the different phases of syn-depositional salt flow.

708 # Figures

709 Figure 1

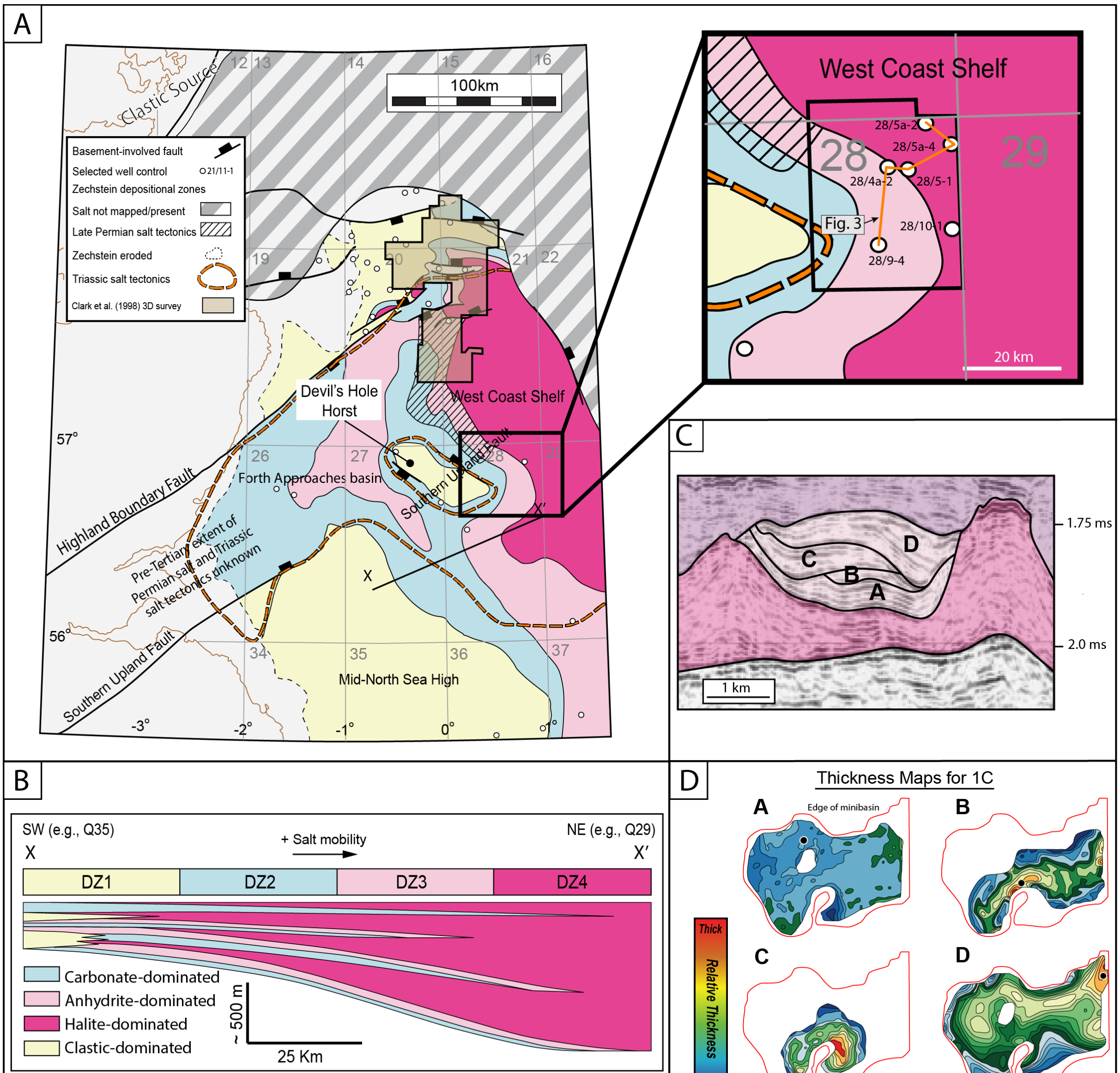


710 * DZ = Depositional Zone

711

Figure 2

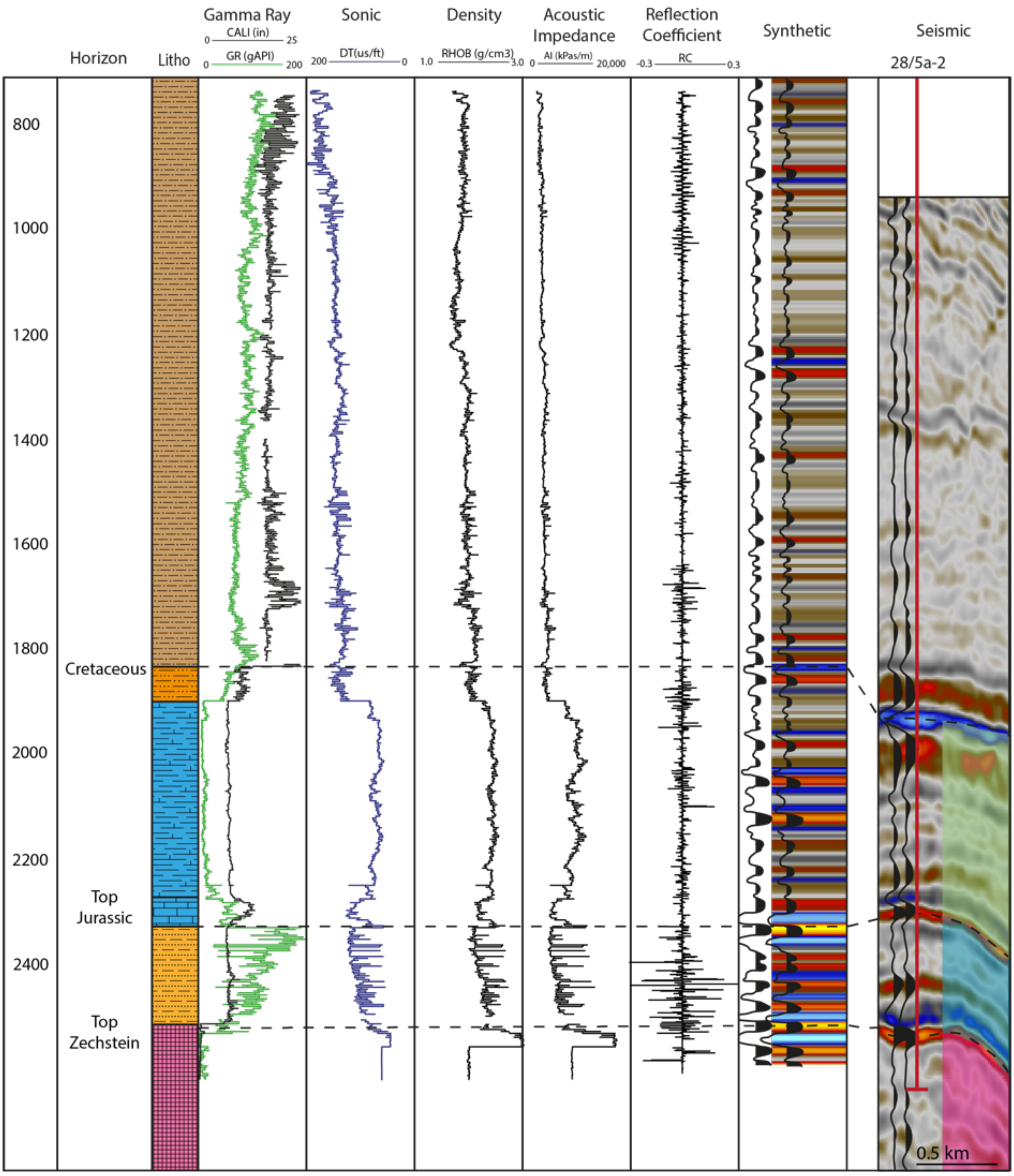
Horizon
Litho
Gamma Ray
CALI (in)
0
25
GR (gAPI)
0
200
Sonic
DT(us/ft)
200
0
Density
RHOB (g/cm3)
1.0
3.0
Acoustic Impedance
AI (kPas/m)
0
20,000
Reflection Coefficient
RC
-0.3
0.3
Synthetic
Seismic
28/5a-2
800
1000
1200
1400
1600
1800
2000
2200
2400
Cretaceous
Top Jurassic
Top Zechstein
0.5 km

714 Figure 3

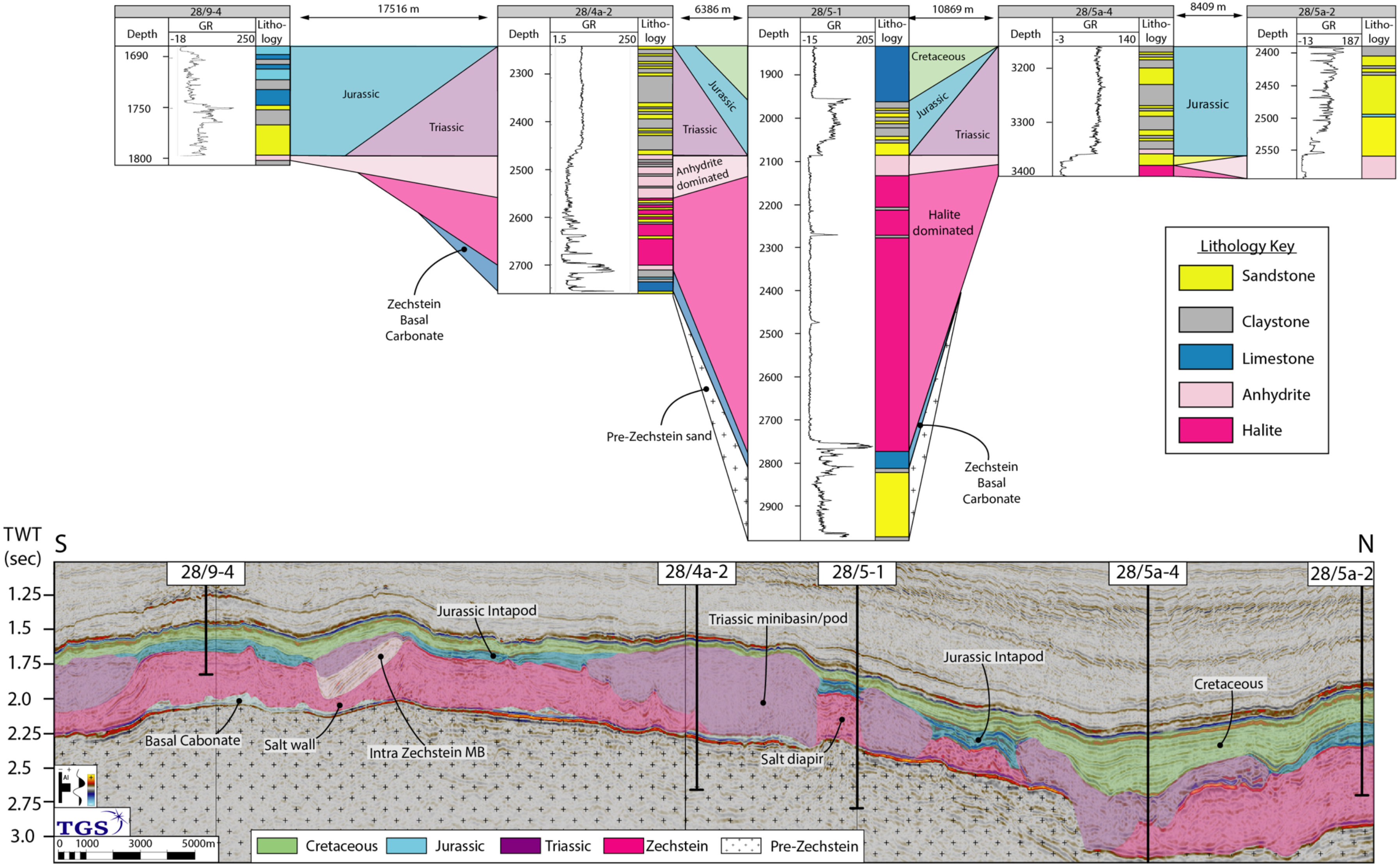


715

716 Figure 4

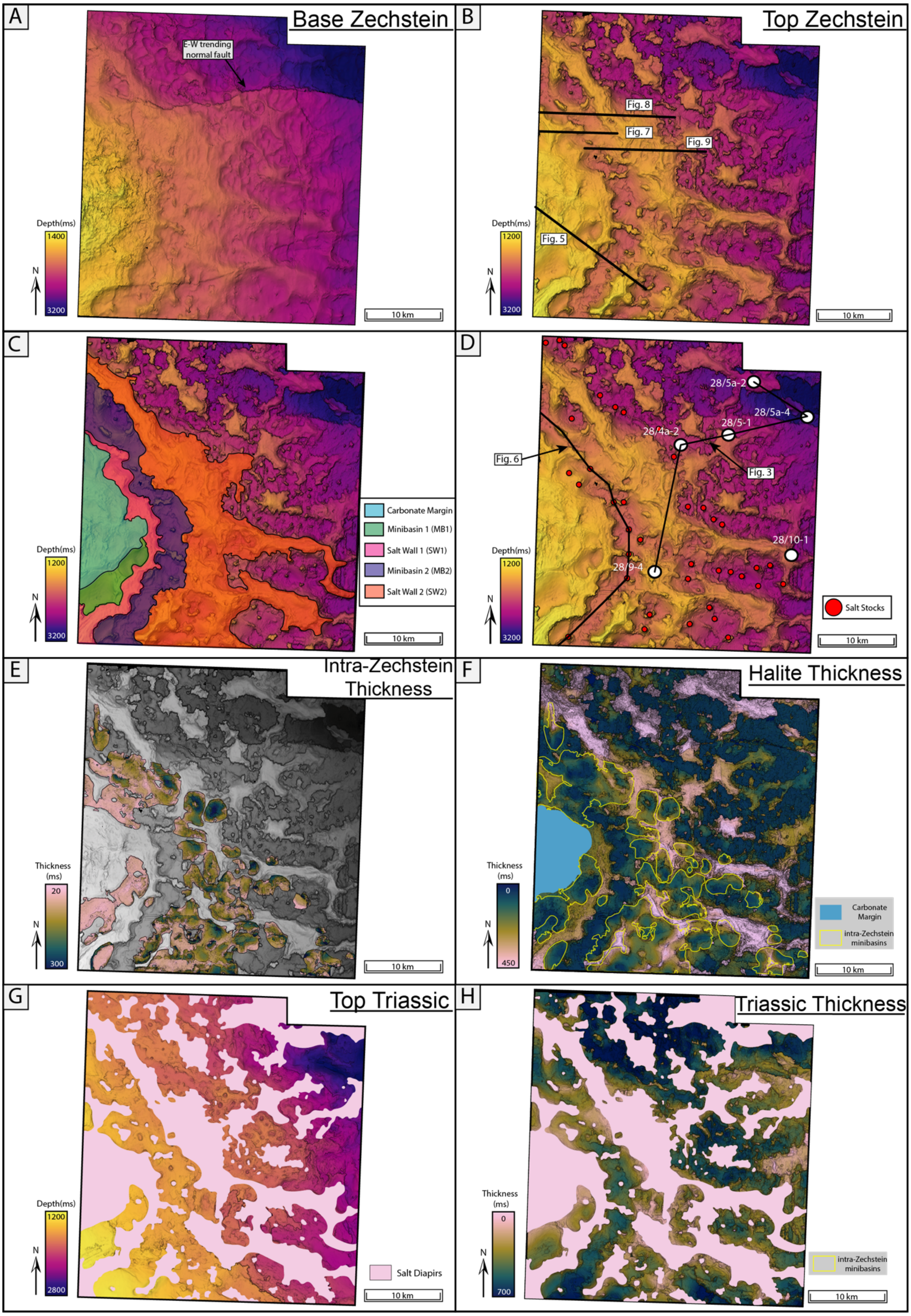


717

718 **Figure 5**

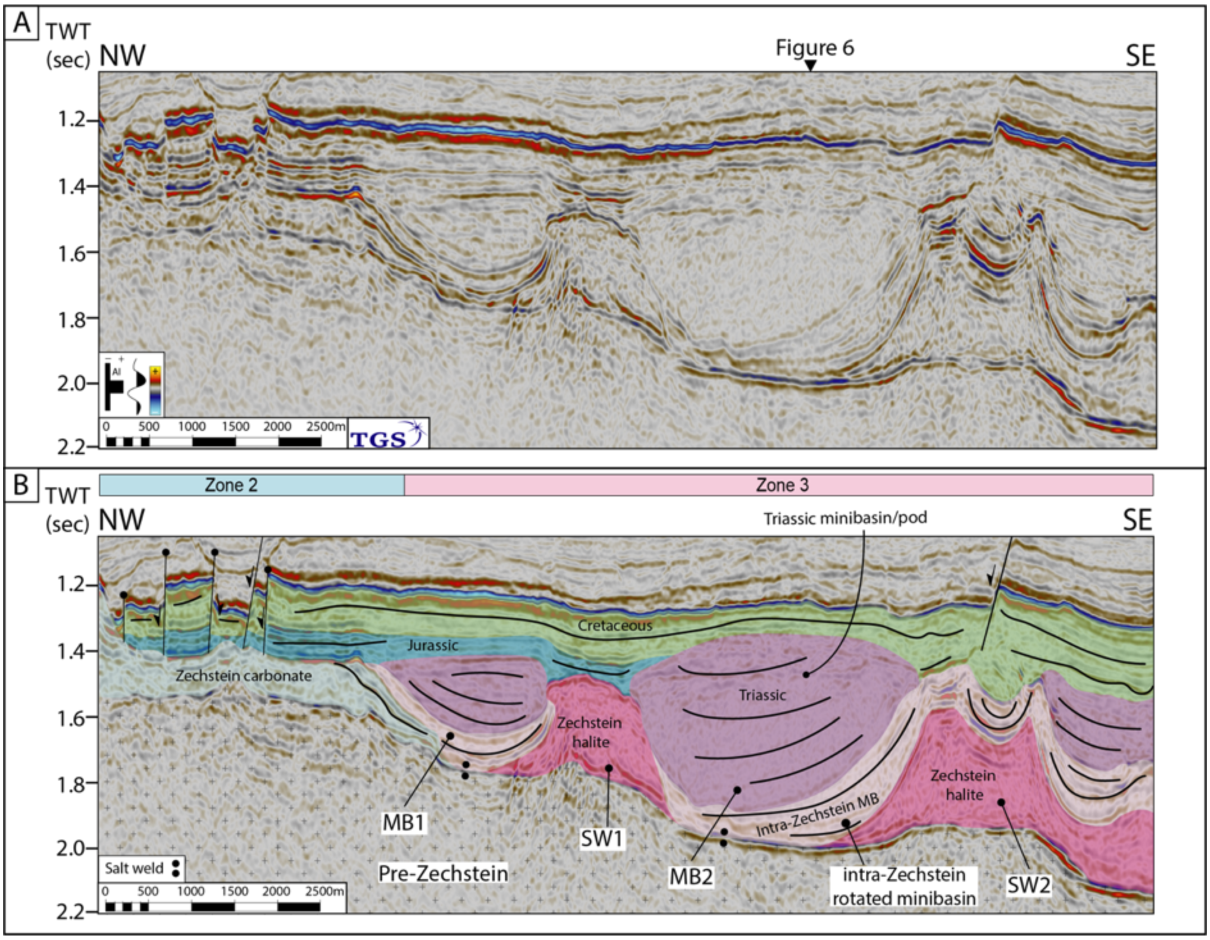


719

720

Figure 6

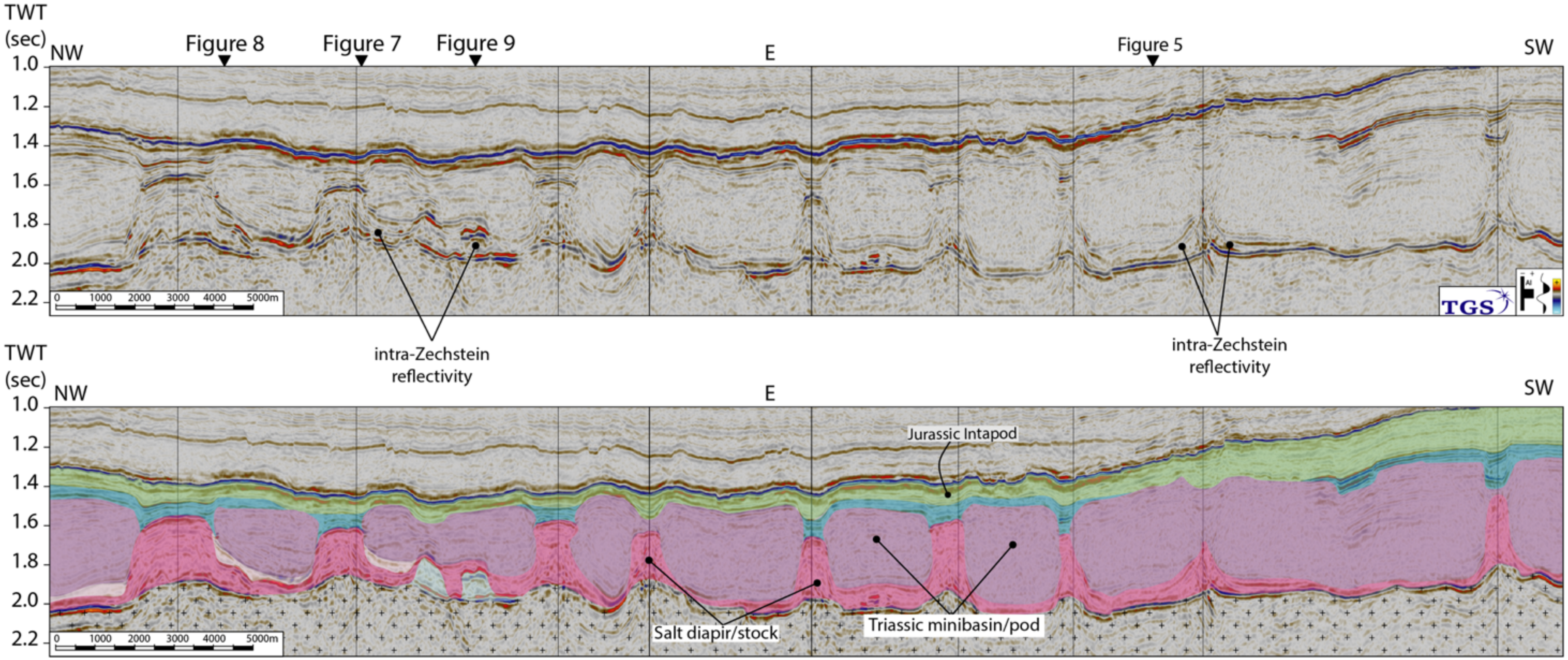

TWT (sec)
NW
Figure 8
Figure 7
Figure 9
E
Figure 5
SW
1.0
1.2
1.4
1.6
1.8
2.0
2.2
0 1000 2000 3000 4000 5000m
TGS
intra-Zechstein reflectivity
intra-Zechstein reflectivity
TWT (sec)
NW
E
SW
1.0
1.2
1.4
1.6
1.8
2.0
2.2
Jurassic Intapod
Salt diapir/stock
Triassic minibasin/pod
0 1000 2000 3000 4000 5000m

724 Figure 7

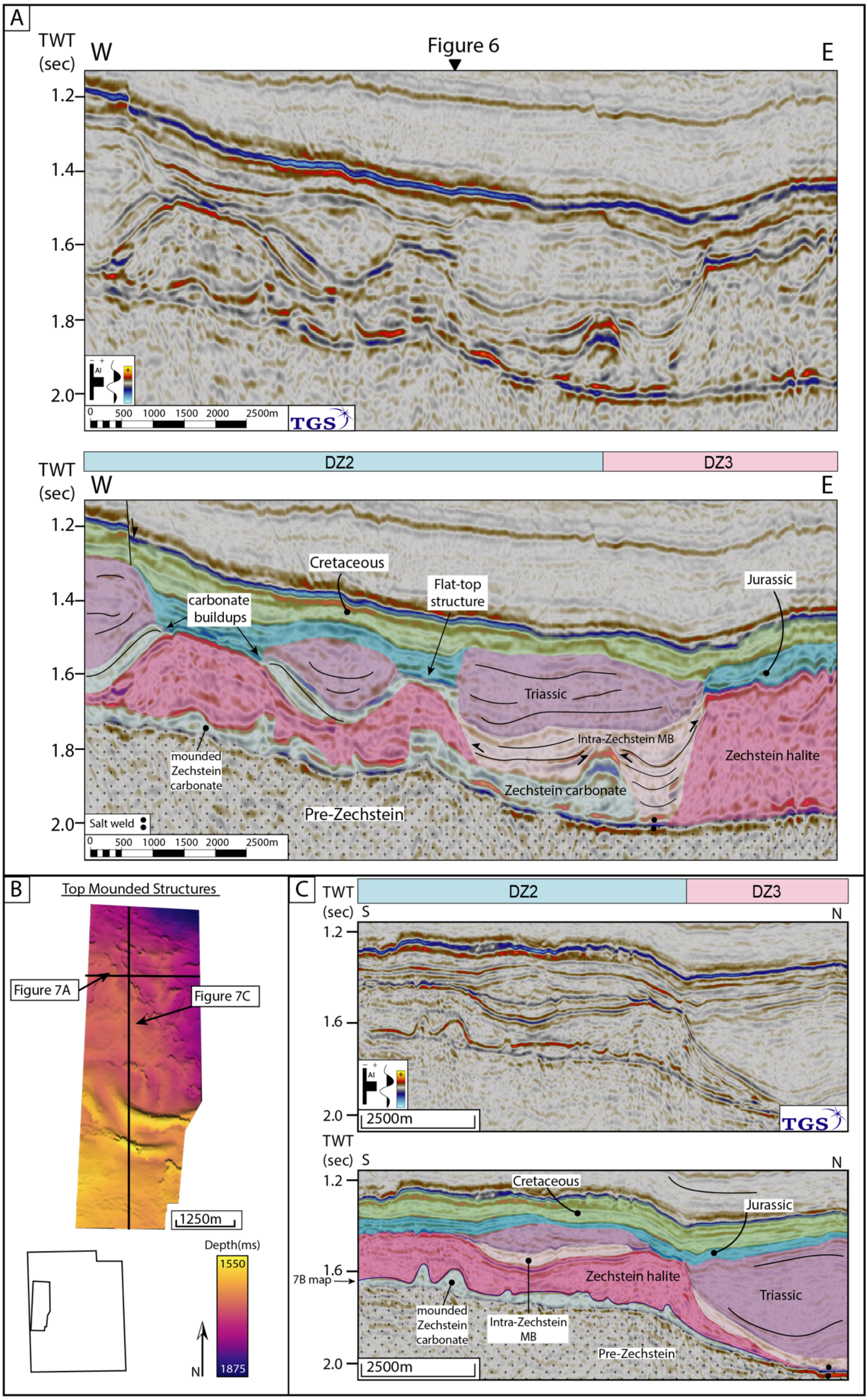


725

726 Figure 8

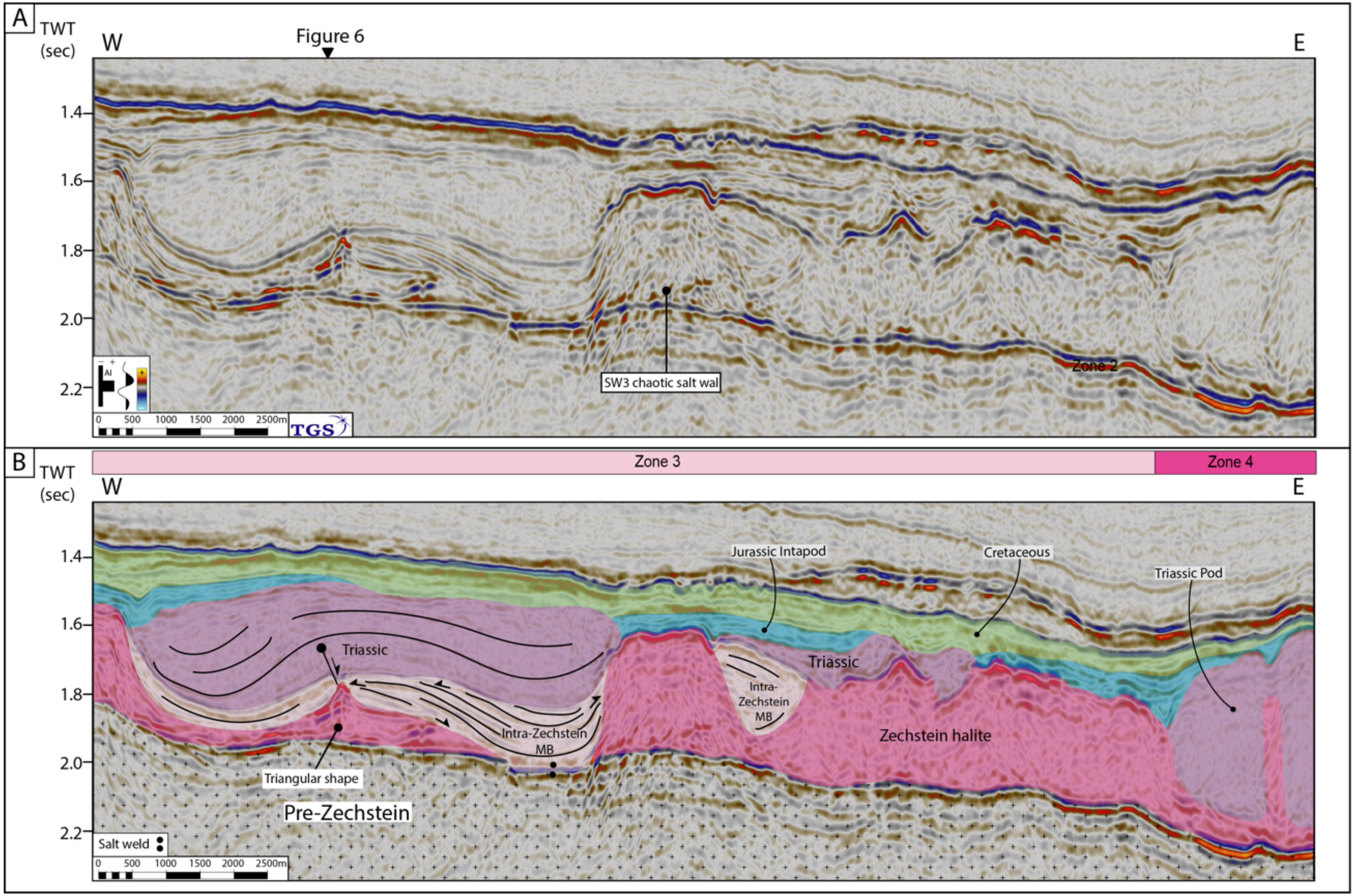


727

728 Figure 9

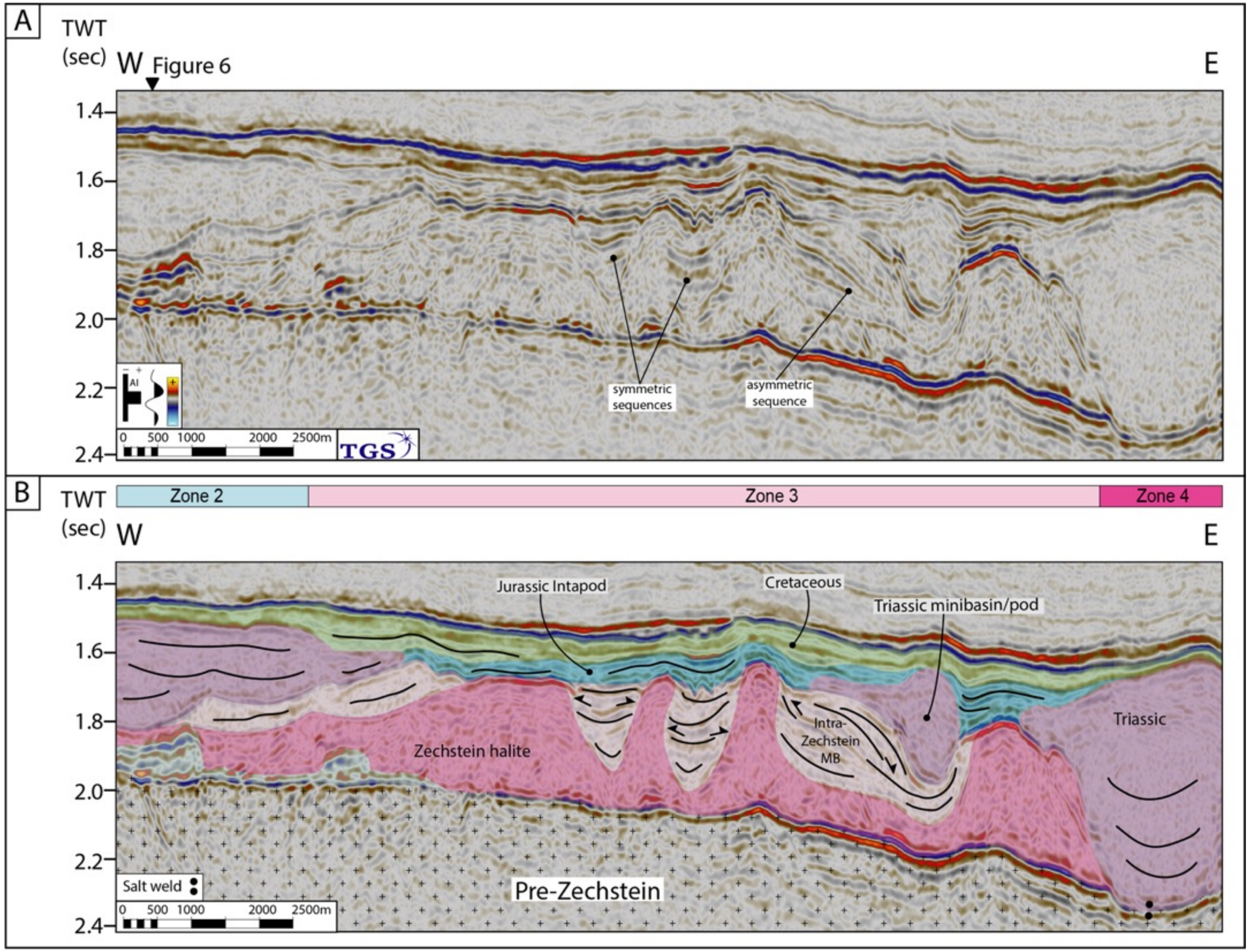


729

Figure 10

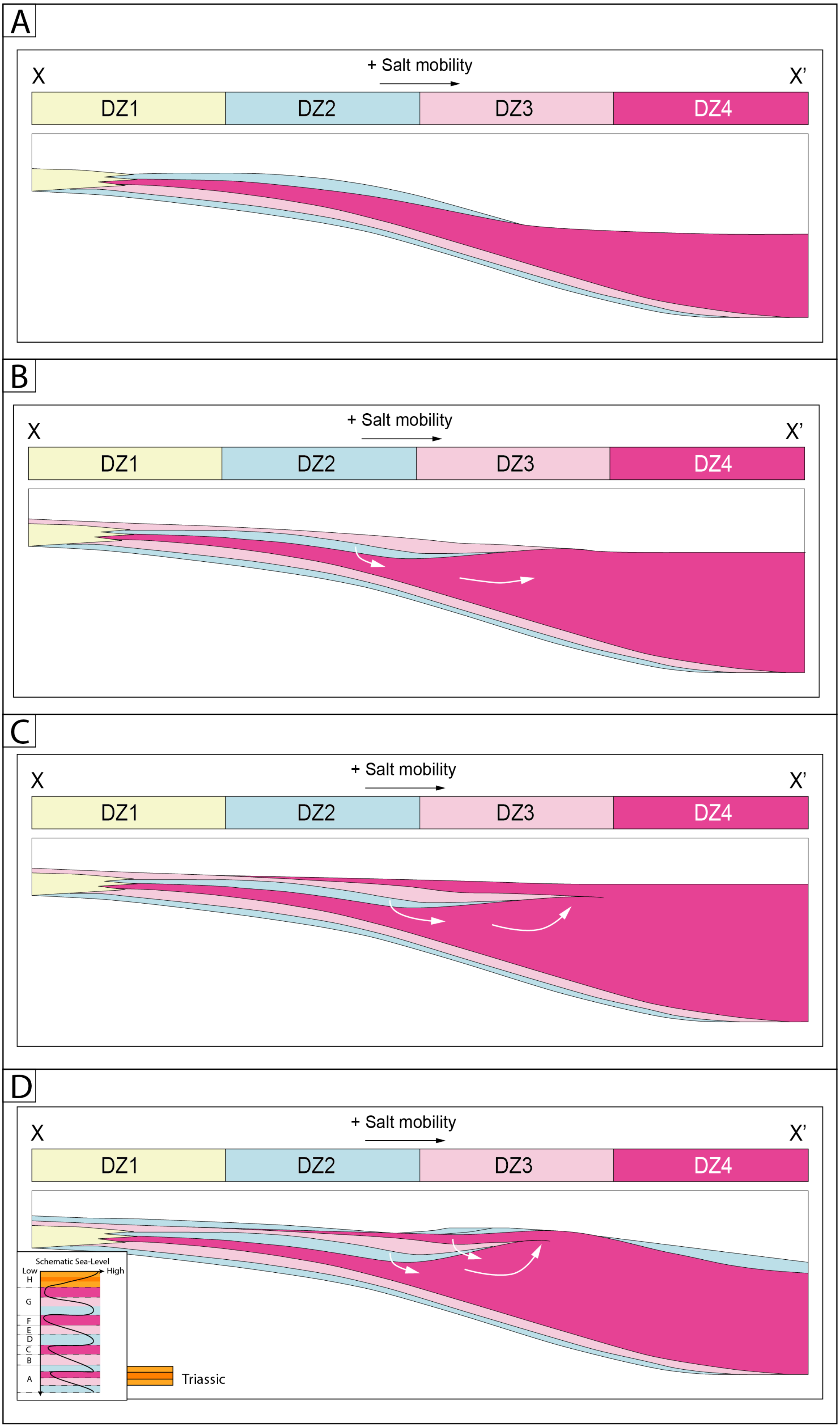
A
+ Salt mobility
X
X'
DZ1
DZ2
DZ3
DZ4
B
+ Salt mobility
X
X'
DZ1
DZ2
DZ3
DZ4
C
+ Salt mobility
X
X'
DZ1
DZ2
DZ3
DZ4
D
+ Salt mobility
X
X'
DZ1
DZ2
DZ3
DZ4
Schematic Sea-Level
Low
High
H
G
F
E
D
C
B
A
Triassic

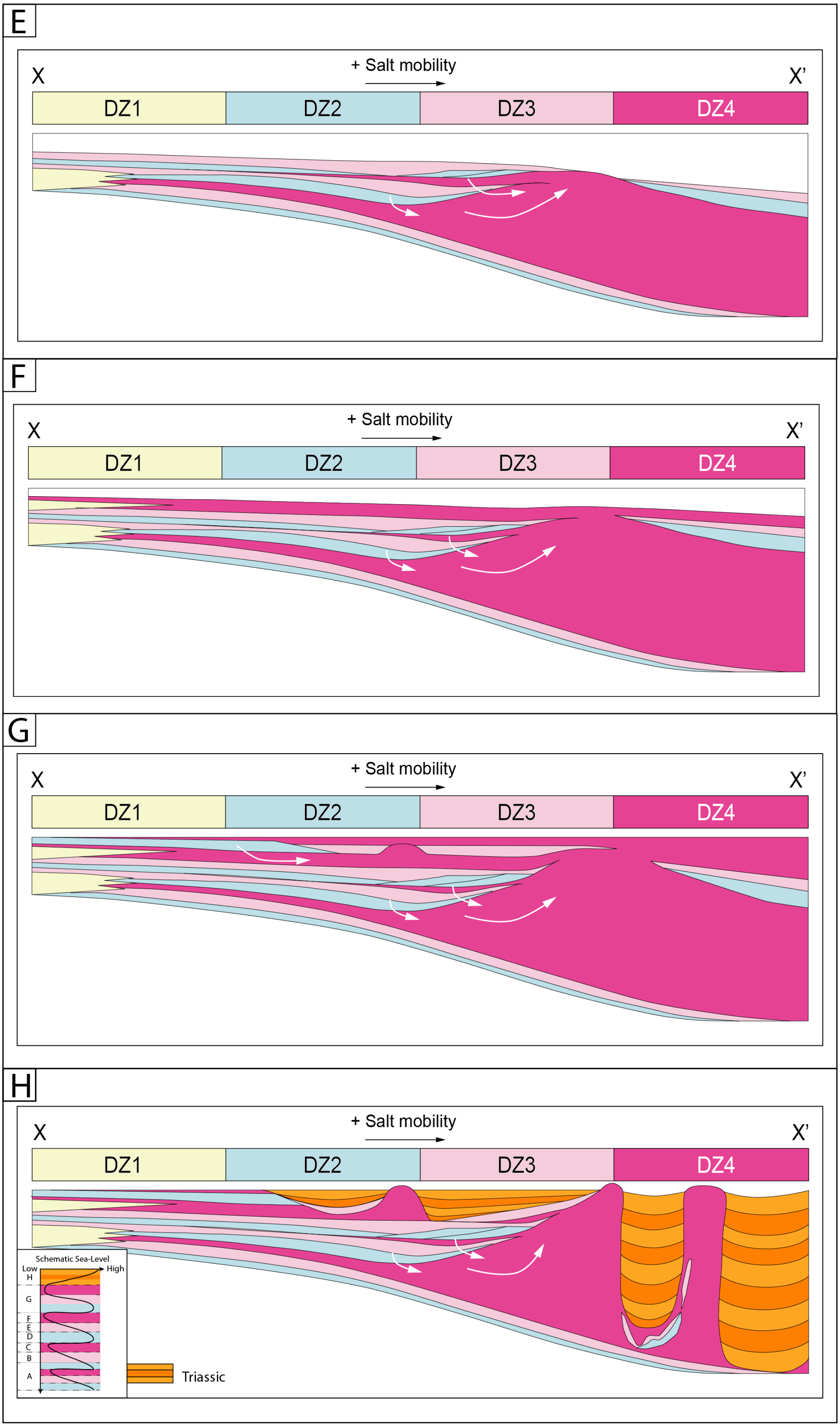
E
X
+ Salt mobility
X'
DZ1
DZ2
DZ3
DZ4
F
X
+ Salt mobility
X'
DZ1
DZ2
DZ3
DZ4
G
X
+ Salt mobility
X'
DZ1
DZ2
DZ3
DZ4
H
X
+ Salt mobility
X'
DZ1
DZ2
DZ3
DZ4
Schematic Sea-Level
Low
High
H
G
F
E
D
C
B
A
Triassic